Lawrence Berkeley National Laboratory
LBL Publications

Title
The Role of Capillary Hysteresis and Pore-Scale Heterogeneity in Limiting the Migration of Buoyant Immiscible Fluids in Porous Media

Permalink
https://escholarship.org/uc/item/8s05s8r3

Journal
Water Resources Research, 54(7)

ISSN
0043-1397

Authors
Cihan, Abdullah
Wang, Shibo
Tokunaga, Tetsu K
et al.

Publication Date
2018-07-01

DOI
10.1029/2018wr022741

Peer reviewed

eScholarship.org Powered by the California Digital Library
University of California

The Role of Capillary Hysteresis and Pore-Scale Heterogeneity in Limiting the Migration of Buoyant Immiscible Fluids in Porous Media

Abdullah Cihan[1], Shibo Wang[1], Tetsu K. Tokunaga[1], and Jens T. Birkholzer[1]

[1] Lawrence Berkeley National Laboratory, Energy Geosciences Division, Berkeley, CA, USA

Correspondence to: A. Cihan, acihan@lbl.gov

Abstract

Understanding the main mechanisms affecting long-term migration and redistribution of injected CO_2 in geological carbon storage is needed for developing predictive models to assess environmental risks and designing monitoring schemes. Preparation of a postinjection site care plan is required for CO_2 injection wells, including monitoring of pressure changes and injected CO_2 plume. Knowledge gaps exist regarding assessment of postinjection monitoring timeframes for the CO_2 plume because the processes driving long-term CO_2 plume migration and trapping are not fully understood. In the postinjection stage of geological carbon storage, redistribution of CO_2 occurs mainly due to buoyancy and capillary forces. This work presents experimental and modeling studies to investigate processes contributing to postinjection plume distribution and stabilization. We conducted a flow cell experiments (0.5 m × 0.05 m × 0.01 m) with two immiscible fluid phases in a glass bead porous medium to study postinjection plume behavior. We employed a hysteretic macroscopic two-phase flow model to interpret the experimental results and to understand main processes leading to plume stabilization. Our findings show that capillary pressure hysteresis explains the experimentally observed plume shape and redistribution at early postinjection stages; however, the long-term plume migration and eventual plume stabilization can only be represented when in addition microscale heterogeneity is accounted for. Results also show that plume stabilization can be extremely slow and that the migration of the plume front can occur through multiple intermittent bursts over long times. Further studies are needed to understand implications of the results for more realistic porous media and large-scale storage reservoirs.

1 Introduction

Understanding main mechanisms affecting the migration and redistribution of injected CO_2 in geological carbon storage (GCS) is necessary to develop predictive models for design and operation of safe storage projects. The U.S. Environmental Protection Agency Class VI permit application for GCS (U.S. Environmental Protection Agency, 2008) requires preparation of a postinjection site care plan including monitoring of pressure changes and injected CO_2 plume. Monitoring is typically required for at least 50 years, but shorter monitoring timeframes and revisions to the postinjection site care

plan may be acceptable if nonendangerment (e.g., sufficient pressure decline and demonstrated CO_2 trapping) to underground sources of drinking water can be demonstrated. However, knowledge gaps exist regarding assessment of postinjection monitoring timeframes for the CO_2 plume because the processes driving long-term CO_2 plume migration and trapping are not fully understood. Experimental and theoretical studies of multiphase flow processes contributing to temporal plume evolution and stabilization can aid in bridging the gaps.

In the postinjection phase of GCS, redistribution of CO_2 occurs mainly due to buoyancy and capillary forces. Until the CO_2 immobilizes, the leading edge of the plume continue to migrate (i.e., drainage), whereas the host rock fluid (e.g., brine) displaces CO_2 in other parts of the plume (i.e., imbibition). Recent experimental and modeling studies show that capillary pressure hysteresis and heterogeneity at different scales control the distribution of fluids during the postinjection phase of CO_2 storage (e.g., Cihan et al., 2017; Doughty, 2007; Juanes et al., 2006; Trevisan et al., 2014, 2015, 2017; Zhao et al., 2013, 2014).

Trevisan et al. (2015, 2017) investigated plume behavior affected by facies-based heterogeneity (centimeter to meter scale) using sandbox experiments with CO_2/brine analog fluids. Their findings show that spatial variability in capillary entry pressures controls the plume migration by causing capillary barriers between the facies with finer and coarser pore sizes. The spatially disconnected facies with relatively lower capillary entry pressures (coarser pore sizes) traversed by an injected CO_2 plume can contribute to long-term trapping of CO_2 by effectively immobilizing the CO_2 during the postinjection phase when pressure gradients diminish. Using the experimental data generated by Trevisan et al. (2015), Cihan et al. (2017) show that neglecting hysteresis in the traditional two-phase flow modeling approach may result in significant overprediction or underprediction of plume evolution and extent.

In addition to macroscale heterogeneity, pore-scale heterogeneities due to variations in pore sizes and geometry can influence the plume evolution. Based on laboratory-scale studies in quasi 2-D flow cells packed with glass beads, Zhao et al. (2013, 2014) suggest that *capillary pinning* and *nose blunting* are the two important processes limiting the migration of a nonwetting fluid plume under buoyancy and capillary-dominated flow conditions. Capillary pinning refers to stabilization of plume due to capillary pressure hysteresis between drainage and imbibition. Zhao et al. (2013, 2014) state that capillary pressure hysteresis eventually causes the cease of the plume movement at a finite distance from the injection location. In addition to capillary pressure hysteresis, variations in capillary entry pressure due to pore-scale heterogeneity and anisotropy further slow the movement of the plume and thicken the plume at the nose, which Zhao et al. (2014) referred to as capillary blunting or nose blunting. Zhao et al. (2014) constructed a sharp-interface model accounting for the effects of capillary pinning and blunting to describe the observations in the flow cell

experiments. A critical parameter, nose height, scaled as a function of the Bond number and the difference between drainage and imbibition capillary pressures, represents the blunting effect as a boundary condition at the nose of the plume. The interface at the nose is pinned (i.e., the flux is zero at the nose of the plume) when the plume thickness is smaller than the critical nose height. Zhao et al. (2014) proposed that capillary pinning could be a potentially important trapping mechanism in addition to structural, residual, and mineral trapping.

Our objective in this study is to investigate two-phase flow processes of immiscible fluids contributing to postinjection plume evolution and stabilization. We conducted a flow cell experiment (0.5 × 0.05 × 0.01 m) similar to those of Zhao et al. (2014) to advance their findings over longer migration times. Our findings demonstrate that the plume stabilization can be extremely slow and that the plume front migrates intermittently through periods of stagnation followed by sudden migration bursts. This can continue over long postinjection times. We also did modeling analyses to obtain insights on the reasons for plume stopping at finite distance from the injection followed by bursts in plume front motion. Differently from Zhao et al. (2013, 2014), we use a two-phase flow continuum model to interpret the experimental findings. The model selected (Cihan et al., 2017) represents hysteresis effects and variations of two-phase flow parameters due to microscale variations in pore sizes and geometry, and as a result, it should naturally represent the blunting effect discussed above.

2 Flow Cell Experiment

Fire-hardened glass beads of spherical shape with 1-mm mean bead size (Propper Manufacturing Co., Inc.) were used as the porous medium material in the experiment. The glass beads were first cleaned by acid washing with 1 M HCl (J.T.Baker®) and then rinsed with a large amount of deionized water (resistivity of 18.2 MΩ/cm, Milli-Q Integral Water Purification System, Millipore Corp). After cleaning, the beads were oven-dried at 110–120 °C and stored in clean capped vessels before use. In the immiscible flow experiment under capillary- and buoyancy-dominated flow regime, we used an air-propylene glycol fluid pair. Air served as the buoyant nonwetting fluid phase, and propylene glycol ($C_3H_8O_2$, anhydrous, 99+% purity, ACROS Organics) was used as the native wetting fluid phase. The experiment was carried out under room temperature and pressure (0.1 MPa, 23.4 ± 0.5 °C). Fluid and interfacial properties of the fluid phases involved in this study are listed in Table 1.

Table 1
Fluid and Interfacial Properties Under the Experimental Conditions

Fluid and interfacial properties	Unit	Value
Propylene glycol density	kg/m^3	1,030[a]
Air density	kg/m^3	1.2
Propylene glycol viscosity	Pa·s	4.2×10^{-2}
Air viscosity	Pa·s	1.9×10^{-5}
Interfacial tension, γ	mN/m	36.0[b]

[a]The propylene glycol density was obtained from the manufacturer (ACROS organics). [b]The interfacial tension value for air-propylene glycol was measured in our laboratory using the KRÜSS Tensiometer.

The dimensions of the acrylic (poly methyl methacrylate) flow cell (Figure 1, length of 56 cm, height of 5.2 cm, and thickness of 1.0 cm) are the same as in Zhao et al.'s (2014) work to facilitate comparison between our results with their study of a similar kind. One end piece was fixed to the other walls, while the opposite end consisted of a removable cap that was bolted to the body of the flow cell. A rubber gasket was used underneath the bolts to create a leak-free system, and a venting port was included near the top of the cell to connect the system with atmosphere pressure. The flow cell and all the components were cleaned with detergent first, followed by ethanol (C_2H_5OH, anhydrous, ≥99% purity, Amresco®) and deionized water rinsing for several times. It was dried by flushing with compressed air.

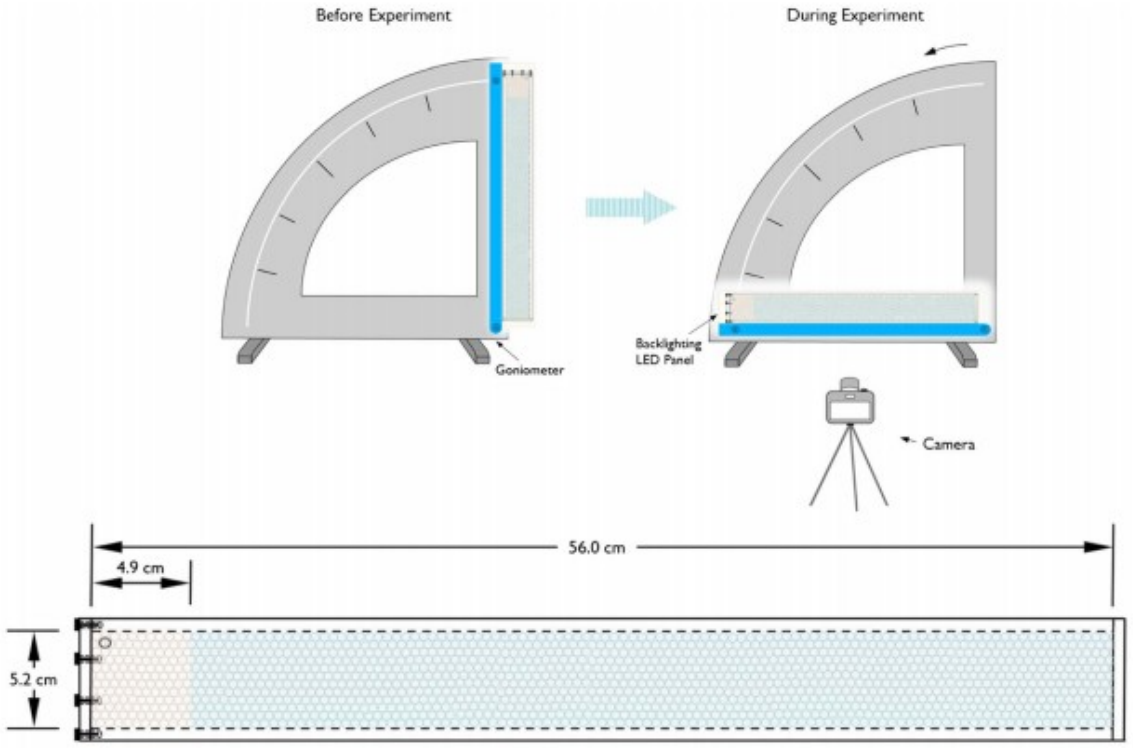

Figure 1

Diagram of flow cell for the gravity exchange flow experiments. In the cavity of the flow cell, the glass beads are wet packed in the native fluid (marked in light blue) and dry packed in the buoyant fluid

(marked in light orange). The lid/cap is sealed into place with bolts through a rubber gasket (not shown). The cell was positioned in the vertical direction before the experiment (left). The cell was rotated into the horizontal direction to start an experiment (right).

We used the wet packing method to achieve an initial complete saturation of the native (wetting) fluid. During the wet packing, the flow cell was set up in the vertical direction. Small amounts of wetting fluid (propylene glycol) were first added to the bottom part of the chamber cavity using a volumetric pipette. Glass beads were then carefully submerged layer by layer into the propylene glycol. Following the same procedure, the addition of propylene glycol and glass beads was alternatively added with glass beads submerged 0.5–1 cm (i.e., about 5–10 layers of beads) below the buoyant-native fluid meniscus before it approached the targeted height of packing (4.9 cm from the cap). The packing above the propylene glycol-air interface was completed by placing glass beads up until the top of the cell was filled. The flow cell was shaken and tapped during the entire packing process to ensure firm and homogenous packing. The packing resulted in two sections with full effective saturations of the buoyant and native fluids (4.9-cm-long air section marked in light orange and 51.1-cm-long propylene glycol section marked in light blue), respectively, as shown in Figure 1.

After the packing of the quasi 2-D flow cell was completed, the cell was installed vertically on a slotted 90° scaled goniometer device made of cast steel, as shown in Figure 1. Prior to the experiment, the air vent port was closed. The cell was rotated counterclockwise and positioned in the horizontal direction to start an experiment (Figure 1). The buoyancy-driven movement of the two immiscible fluid phases was thus initiated, resulting in the propylene glycol and air phases migrating in a countercurrent manner.

Separate measurements were performed to determine the porosity and permeability of the wet-packed porous media and capillary pressure-saturation functions. Porosity was measured to be about 40% using a volumetric method. The permeability was determined to be about 7.6×10^{-10} m^2 using the falling head method (Klute & Dirksen, 1986).

The capillary pressure (P_c)-saturation (S_w) measurements with propylene glycol-air were conducted using the porous plate (*hanging column*) method (Tokunaga et al., 2002). The homogeneous glass beads were packed inside an acrylic ring on top of the porous plate forming the sample column (diameter = 92 mm, height = 30 mm, porosity $\varphi \approx 0.38$, pore volume = 63.0 ml). Figure 2a shows the measured primary drainage and main wetting functions (filled circles: red for drainage and blue for imbibition).

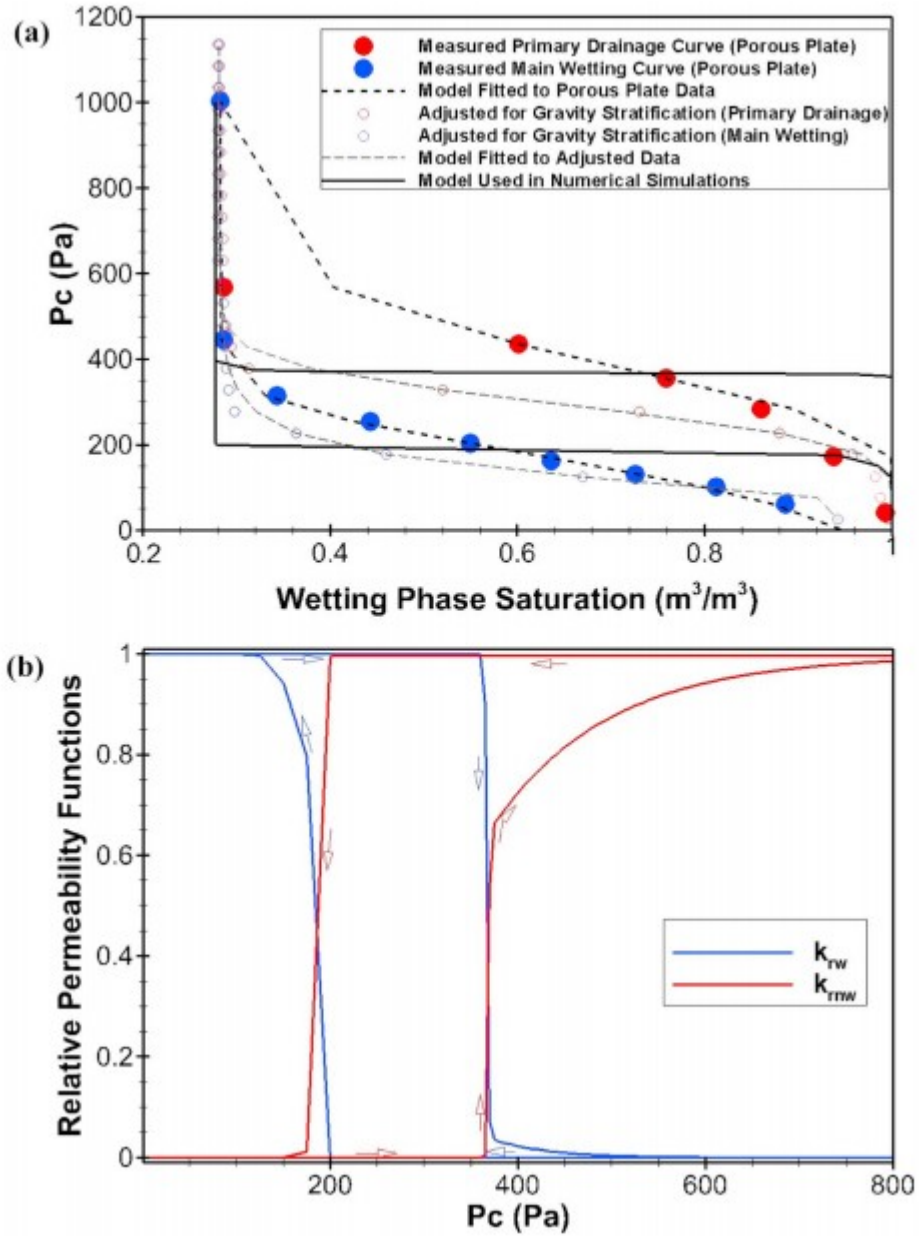

Figure 2

Fitted and adjusted hysteretic P_c-S_w-k_{rw}-k_{rn} functions of primary drainage and main wetting processes for air-propylene glycol fluid pair in a 1-mm-glass bead porous medium. Sharp functional relationships are used in the numerical simulations to represent the observed sharp transition zone between the fluids in the experiments (Figures 4 and 5).

3 Modeling Approach

We used traditional two-phase flow model equations with hysteretic constitutive models as given by Cihan et al. (2017) to interpret the experimental findings and investigate the main processes controlling the plume migration. Cihan et al. (2014) introduced the drainage connectivity function, $P^d(r, P_c)$, and the wetting connectivity function, $P^w(r, P_c)$, together

with a probability distribution function, $f(r)$, for void volume fraction to mathematically represent hysteresis in the saturation-capillary pressure (S_w-P_c) function. $P^d(r, P_c)$ is defined as the cumulative ratio of drained volume of r-sized voids with wetting fluid phase at a given capillary pressure P_c relative to the total volume of r-sized voids. $P^w(r, P_c)$is defined as the cumulative wetted (or imbibed) volumetric ratio of r-sized voids at P_c relative to the total volume of r-sized voids. The following nonlinear Gaussian cumulative functions represent $P^d$and P^w (Cihan et al., 2014):

$$\mathbf{P^d}(r,P_c) = a_d\,0.25\left[1+\operatorname{erf}\left(\frac{P_c-b_d}{\sqrt{2}c_d}\right)\right]\left[1+\operatorname{erf}\left(\frac{r/r_{\max}-d_d}{\sqrt{2}e_d}\right)\right]\Phi[P_c-P_d(r)] \quad (1)$$

where Φ [ ] is the unit step function, and

$$\mathbf{P^w}(r,P_c) = a_w\,0.25\left[1-\operatorname{erf}\left(\frac{P_c-b_w}{\sqrt{2}c_w}\right)\right]\left[1-\operatorname{erf}\left(\frac{r/r_{\max}-d_w}{\sqrt{2}e_w}\right)\right]\Phi[-P_c+P_w(r)] \quad (2)$$

where a, b, c, d, e with (d, $e\in[0,1]$) are constants with subscripts (d, w) for drainage and wetting. $P_d(r)$ and $P_w(r)$ represent the threshold capillary pressures obtained based on Young-Laplace equation for entry of fluids into voids during drainage and wetting (or imbibition), respectively. $f(r)$ is represented by a generalized lognormal distribution,

$$f(r) = \frac{1}{\sqrt{2\pi}\ln\sigma}\exp\left[-\left(\frac{\ln(r'/\mu)}{\sqrt{2}\ln\sigma}\right)^2\right] \quad (3)$$

where $r' = (r - r_{\min})(r_{\max} - r_{\min})/(r_{\max} - r)$, $r_{\max}$ is the maximum void size, and σ and μ are the statistical parameters characterizing the probability distribution of r'. Based on the functional relationships (1–3), Cihan et al. (2017) developed the hysteretic relative permeability ($k_{rw} = k_w/k$, $k_{rn} = k_n/k$) functions for nonwetting and wetting fluids. Detailed descriptions of the hysteretic constitutive models can be found in Cihan et al. (2014, 2017). The relative permeability models contain the unit step functions $\Phi[S_n - S_{cn}]$and $\Phi[S_w - S_{cw}]$ where S_{cn} is the critical saturation for the percolation threshold of the nonwetting fluid in the porous medium and S_{cw} is the critical saturation for the percolation threshold of the wetting fluid. The unit step functions are employed in the models to represent zero permeability in a direction that the fluid does not percolate through the domain. In this study, both S_{cn} and S_{cw} ($\sim\phi_c/\phi$) are set to 0.077 based on van der Marck (1996) who computed void percolation threshold ($\phi_c = 0.03 \pm 0.002$ in 3-D) in randomly packed sphere packings. Based on our sensitivity analyses with the numerical model, those critical saturation parameter values do not have significant influence on velocity and final extent of the plume, but they slightly increase the magnitude of the bursts in plume front movement.

The S_w-P_c functions for primary drainage and main wetting processes were fitted to the data obtained through the porous plate method to estimate the model parameters in equations 1–3 for both hysteretic S_w-P_c function and hysteretic k_{rw} and k_{rn} functions. However, the numerical simulations (2.5 × 2.5-mm resolution) with the fitted functions (Figure 2a, dashed lines) based on the porous plate data (~92 × 30-mm resolution) cannot produce the sharp fluid displacements observed in the experiments. As recognized by earlier studies (e.g., Liu & Dane, 1995; Sakaki & Illangasekare, 2007; Tokunaga et al., 2002), the averaged saturation measurements over the sample columns result in smoothed S_w-P_c curves due to the effect of gravity. The differences between the averaged measurements and local or physical point measurements can be significant especially for measurements in coarse porous media and low interfacial tensions as in this work. However, even when we use the modified data for gravity stratification (based on the procedure in Tokunaga et al., 2002), the numerical model could not appropriately represent the sharp fluid displacements. Therefore, we further adjusted the hysteretic model parameters $P^d$and $P^w$to model the sharp saturation changes observed in the experiment. The solid black lines in Figure 2a represent the primary drainage and main wetting functions based on the adjusted hysteretic model parameters (Table 2). Figure 2b also presents the estimated relative permeability functions for primary drainage and main wetting processes based on the model by Cihan et al. (2017). Note that the constitutive model here does not take into account the contribution of the connected thin wetting films around the glass beads to the relative permeability of the wetting phase at low wetting fluid saturations.

Table 2
Hysteresis Model Parameters Used in the Numerical Simulations

Parameter	Value
Void-volume fraction distribution	
r_{min} (m)	0.00
r_{max} (m)	4.08×10^{-4}
μ (m)	1.87×10^{-4}
σ (m)	1.85
Drainage connectivity function	
P_{dmin} (Pa)	95.68 ($\pm P_{dmin}$ × 5.5%, 6% or 7%)
b_d (Pa)	367.68 ($\pm b_d$ × 5.5%, 6% or 7%)
c_d (Pa)	0.02
d_d (-)	0.24
e_d (-)	1.00×10^{-5}
Wetting connectivity function	
b_w (Pa)	186.62 ($\pm b_w$ × 5.5%, 6% or 7%)
c_w (Pa)	1.26
d_w (-)	0.93
e_w (-)	2.96×10^{-4}

Note. The parameter values of the hysteretic S_w-P_c model for the propylene glycol and air fluid pair were adjusted to represent sharp saturation changes in the flow cell experiment. We obtained the parameters of the void-volume fraction distribution in equation (3) from the model developed by Alonso et al. (1995) for random packing of equal-sized spheres. ($a_d = a_w = 1$).

The hysteretic two-phase flow model equations are discretized numerically by the Finite Volume method (see Cihan et al., 2017, for detailed description of the numerical model). We used a uniform grid size of 2.5 mm × 2.5 mm in a 2-D domain. We run the hysteretic two-phase flow model with and without the effect of microscale variations and compare against the experimental observations to assess whether hysteresis only or hysteresis plus pore-level heterogeneity can explain the observed stagnation of the plume. One can also use pore-network type modeling approaches that can more explicitly represent void space topology and pore-level displacements (e.g., Zhang et al., 2000), although the dimensions of the experimental domain could be too large to compute the pore-network-type models with hysteresis. The purpose of the numerical simulations in this work is to understand the main processes controlling plume evolution and stabilization, rather than perfectly matching the experimental data. Therefore, we followed a simple approach to assess the effects of pore-level heterogeneities due to random packing of beads and variations in bead size, shape, and void geometry. We created small random variations (percent changes around mean of a parameter value) in the hysteretic model parameters assigned for each grid block of the numerical model. We varied only the three parameters ($P_{d\min}$, b_d, b_w) influencing the capillary entry pressures for nonwetting and wetting fluids. We created 10 numerical model realizations for each of the three variation percentages (5.5%, 6%, or 7% percent). Every single grid of the 10 numerical model domains contains randomly assigned values of the three hysteretic model parameters based on a uniform distribution. The impact of the selected variation percentages is presented in section 4.

4 Results

Figure 3 presents the measurements of air plume position as a function of time. Our observations over a 6-month duration demonstrate that after a fast migration period at very early times ($t < 10^{-2}$ d), the plume movement continues very slowly through intermittent bursts of the front position until apparent stabilization of the plume front is achieved ($t \sim 60$ d). The figure also shows qualitatively the resemblance of the early time data between this work and Zhao et al. (2014). Both data sets were obtained under similar conditions (Bo, Bond number) except that Zhao et al.'s (2014) measurements in Figure 3 were obtained in a slightly coarser glass bead medium. Note that Zhao et al. (2014) show that the lateral extent of the plume decreases with increasing Bo^{-1}. This trend does not appear in the two data sets in Figure 3. The reason could be due to some differences between the experimental procedures followed here and in Zhao et al. (2014). However, Figure 3 indicates the importance of conducting the experiments for longer time periods to ensure that the intermittent behavior with periods of bursts and stagnation are not mistaken for long-term final plume stabilization.

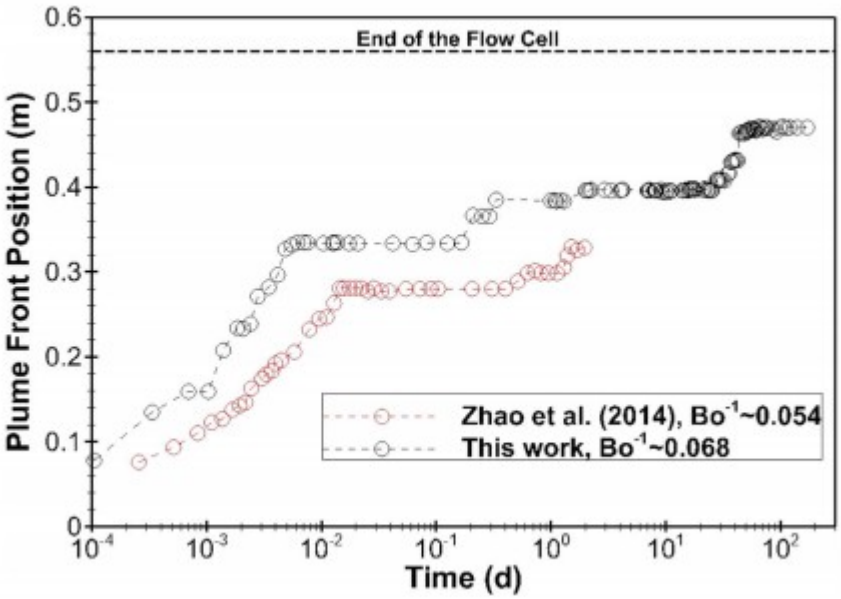

Figure 3

Time evolution of air plume front position in a propylene glycol-saturated porous medium. $Bo^{-1} = \gamma/(d \times \Delta\rho \times g \times H)$, where $\Delta\rho$ is density difference between the propylene glycol and air, d is the mean glass bead diameter, g is the gravitational acceleration, and H is the height of the flow cell.

After the initiation of the buoyancy-driven movement of the two immiscible fluid phases, the nonwetting fluid starts to displace the wetting fluid laterally at the top (drainage) while the wetting fluid displaces the nonwetting fluid at the bottom (imbibition; Figure 4a). As observed by Zhao et al. (2013, 2014), a portion of the initial vertical interface below the drainage zone is pinned. Zhao et al. (2013, 2014) state that the capillary pressure hysteresis between drainage and imbibition is the reason for pinning of the interface and the cease of the plume movement. The thickness of the pinned vertical interface decreases with time as the imbibition front at the bottom of the source zone continues moving upward. However, the pinned vertical interface never vanishes, producing a distinctly different plume thickness at the source zone compared to the rest of the plume under macroscopically homogenous conditions. Eventually the plume stops moving at a finite distance before reaching the lateral boundary (Figures 4a and 5a). It is worth noting that at equilibrium the vertical distance between the pinned interfaces at the source zone and at the nose of the plume is approximately equal to the difference between the drainage and the imbibition capillary threshold pressure heads (Figure 2a). As indicated by Zhao et al. (2014), the migration behavior with pinning/depinning and plume stopping at a finite distance is in contrast with the indefinite spreading of buoyancy-driven miscible fluids (e.g., Huppert & Woods, 1995). In addition, based on our own modeling studies, the traditional two-phase flow model without hysteresis effects completely fails to represent the observed behavior in the experiments.

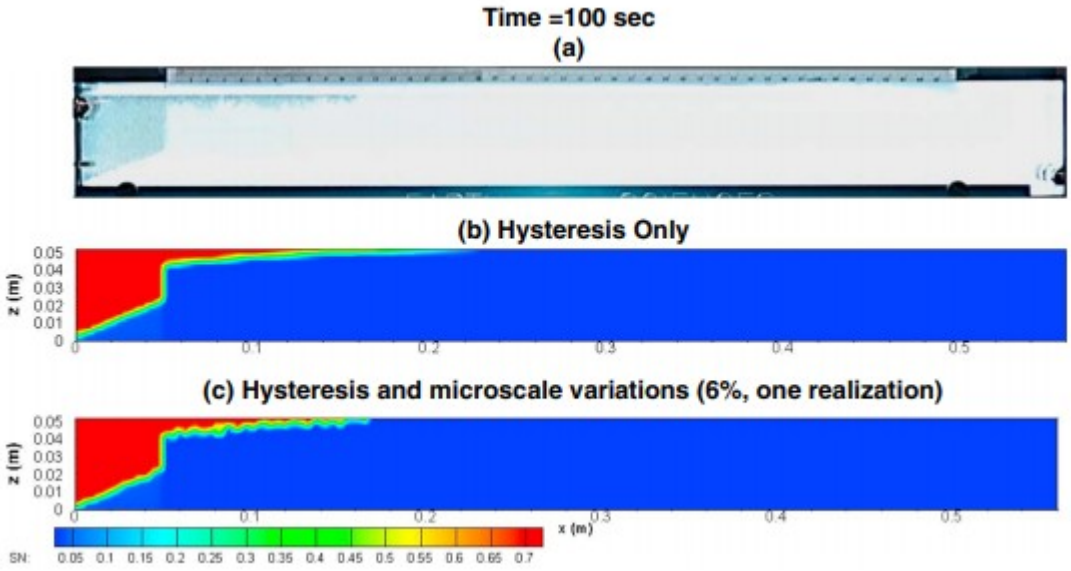

Figure 4

An early time postinjection distribution of the nonwetting fluid plume (100 s): Hysteretic two-phase flow model results without (b) and with (c) variations in the model parameters.

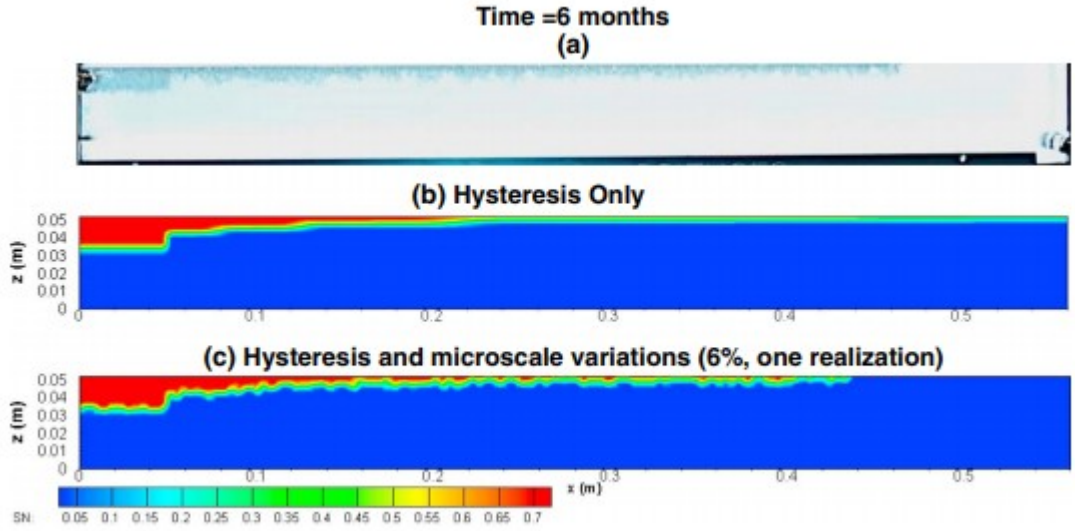

Figure 5

Final distribution of the nonwetting fluid plume (6 months): Hysteretic two-phase flow model results (b) without and (c) with variations in the model parameters.

We employed the hysteretic two-phase flow model to gain insights on pinning of the interface, the cease of the plume movement, and occurrence of intermittent bursts. The hysteretic model successfully produced the pinning/depinning behavior at very early times ($t < 10^{-2}$ d; Figure 4b). However, according to our modeling analyses, hysteresis alone in a homogeneous porous medium cannot explain the observed plume stabilization before it reaches the flow cell boundary. In contrast, the

simulations accounting for coupled effects of hysteresis and microscale variations, represented by random changes in hysteresis model parameters, represent the cease of the plume movement at a finite distance very well (Figure 5c).

Based on the two-phase modeling studies for interpreting the experimental data, we may conceptually describe our understanding of long-term postinjection behavior of plume migration as follows. As the driving force, buoyancy makes the lighter nonwetting fluid move upward, such that the capillary pressure at the bottom of the source zone decreases, while the capillary pressure toward the top of the source zone increases slightly at the beginning. A capillary pressure profile decreasing from top to bottom develops along the source zone. If the capillary pressure at the top interface between the fluids becomes higher than the capillary entry pressure (drainage threshold) for the nonwetting fluid to invade, the nonwetting fluid starts to displace the wetting fluid from the top of the source zone, leading to lateral plume spreading. Meanwhile, at the bottom, the wetting fluid starts to fill the pore space emptied due to the upward movement of the nonwetting fluid as the capillary pressure (pressure difference at the fluid-fluid interface) becomes less than the wetting fluid entry pressure (imbibition threshold capillary pressure).

As the nonwetting fluid continues to spread, more wetting fluid imbibes from the bottom parts of the plume, pushing the sharp interface at the bottom upward, which causes the effect of the driving force, buoyancy, to decrease. As the displacement continues, the maximum capillary pressure in the system decreases, and eventually the plume can come across a material zone with a higher entry pressure than the capillary pressure (pressure difference) present at the interface. At that instance, the nose of the laterally migrating buoyant plume cannot move unless additional nonwetting fluid accumulates due to continued displacement of nonwetting fluid from the source zone via imbibition and buoyancy. While internally dynamic displacement of the fluids can happen, the plume front can appear stagnant for long times. After a long stagnation period, the plume front can suddenly move when the pressure difference exceeds the capillary entry pressure (Figure 6). Successive stopping and sudden movements can continue for long times, with multiple intermittent bursts. Without microscale variations, according to the two-phase flow model, the plume would continue to move until either the plume reaches the flow cell boundary (Figure 5b) or the saturation throughout the plume becomes less than the residual saturation.

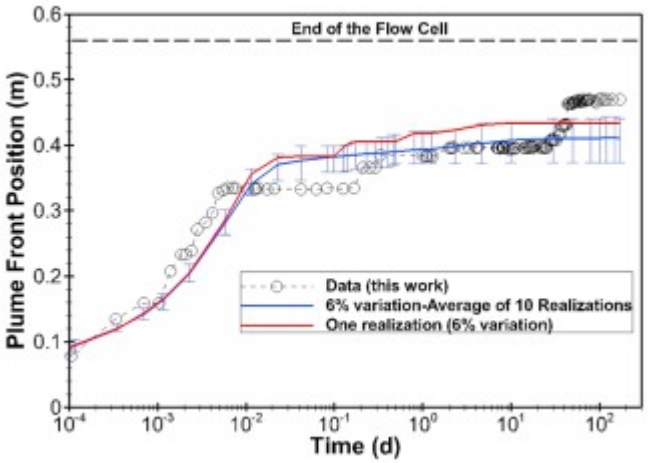

Figure 6

A comparison of the hysteretic two-phase flow model prediction (for 6% variation) against experimental measurements for the evolution of the plume front position. The model results for one realization (red line) appear to show the multiple small bursts of the plume mobilization. Error bars indicate variability in the predicted plume front positions from 10 realizations.

As the buoyancy force decreases due to upward movement of the imbibing interface, the capillary pressures start to equilibrate in the system. At the time of complete plume stabilization, imbibition becomes dominant over the entire extent of the plume. The pressure difference at the nose of the plume is smaller than the capillary entry pressure of the nonwetting fluid, while the pressure difference at the other parts of the nonwetting fluid plume, where imbibition could occur, is higher than the imbibition entry pressure of the wetting fluid, so that wetting fluid cannot imbibe anymore.

Figure 6 shows a comparison of the time evolution of the plume front between the experimental measurements and the hysteretic two-phase flow model prediction with 6% parameter variation. Although most realizations of the model show single or multiple bursts of the plume movements until the plume completely stops (e.g., red line in Figure 6), the magnitudes of the predicted intermittent bursts were not as high as the observed bursts in the experiments. Error bars indicate variability in the predicted plume front positions from 10 realizations. Figure 7 shows that variability in the predicted plume front positions increases with increasing parameter variations. In addition, as the parameter variation increases, the velocity and the lateral extent of the plume decrease because of the increased random heterogeneity. Overall, the two-phase flow modeling analysis in this work indicates that in order to represent the intermittent plume movement observed during the postinjection period, the model must include variations in entry capillary pressure values (hysteretic parameters) due to microscale variations in pore size and geometry.

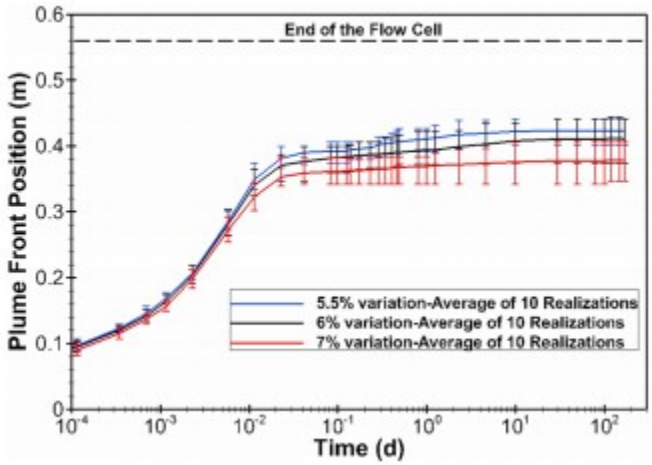

Figure 7

Time evolution of the plume front position affected by parameter variations. As the heterogeneity increases due to increasing variation percent in parameters, the plume stabilizes at shorter distances. Error bars indicate variability in the predicted plume front positions from 10 realizations.

5 Discussion and Conclusions

This study presents experimental and modeling analyses to understand long-term migration behavior of immiscible fluids in application to the postinjection phase of GCS. The experimental results in a macroscopically homogeneous porous medium show that the buoyant plume stops at a finite distance before the entire plume reaches a macroscopic residual saturation. Therefore, this mechanism, referred as capillary pinning, is different from the residual trapping mechanism well known in GCS. The results also show that in long postinjection times, the migration of the plume occurs mainly through intermittent bursts.

The traditional two-phase flow model without hysteresis effects completely fails to represent the observed behaviors in the experiments. Interpretation of the experimental results using a hysteretic two-phase flow model indicate that the coupled effects of capillary hysteresis and microscale heterogeneity can explain the cease of the plume movement and occurrence of the intermittent bursts. Microscale heterogeneity exists in the experiments due to random packing and variations in grain size and geometry. Model simulations considering hysteresis can represent the pinning of the interface at the source zone but cannot account for the stopping of the plume movement at a finite distance. We take into account the microscale heterogeneity by assigning small random variations in the hysteretic capillary pressure-saturation model parameters.

The hysteretic two-phase flow model predicts reasonably well the main features observed in the postinjection plume evolution. However, the magnitudes of the predicted intermittent bursts are not as large as the observed bursts in the experiments. The discrepancy might be due to inaccurate representation of microscale processes and variations in the

macroscopic model. In addition, the constitutive models involve a number of assumptions, one of which is the neglect of wetting film flow contribution at low wetting fluid saturations. The film flow can occur through connected pendular rings around the glass beads at low wetting fluid saturations (Tokunaga, 2009) and can result in snap off of the nonwetting fluid in pore space, and this could enhance stagnation of the nonwetting plume during imbibition (Unsal & Moulet-Vargas, 2013).

Although the density and viscosity ratios of the fluids used in this study are significantly different from those of $scCO_2$-brine, the results of this work investigating long-term basic immiscible displacement processes under capillary- and buoyancy-dominated conditions are relevant for CO_2 storage. Future studies need to address the potential implications of the capillary hysteresis, microscale heterogeneities, and intermittent bursts on the plume evolution and stabilization in more realistic and larger-scale porous media systems.

Acknowledgments

This work was funded by the Assistant Secretary for Fossil Energy, National Energy Technology Laboratory, National Risk Assessment Partnership, of the U.S. Department of Energy at Lawrence Berkeley National Laboratory, under U.S. Department of Energy contract DE-AC02-05CH11231. All data from this study are available in the supporting information and at https://doi.org/10.5281/zenodo.1253266.

References

Alonso, M., Sainz, E., Lopez, F. A., & Shinohara, K. (1995). Void-size probability distribution in random packings of equal-sized spheres. *Chemical Engineering Science*, 50(12), 1983– 1988. https://doi.org/10.1016/0009-2509(95)00061-9

Cihan, A., Birkholzer, J., Illangasekare, T. H., & Zhou, Q. (2014). A modeling approach to represent hysteresis in capillary pressure-saturation relationship based on fluid connectivity in void space. *Water Resources Research*, 50, 119– 131. https://doi.org/10.1002/2013WR014280

Cihan, A., Birkholzer, J., Trevisan, L., Gonzalez-Nicolas, A., & Illangasekare, T. (2017). Investigation of representing hysteresis in macroscopic models of two-phase flow in porous media using intermediate scale experimental data. *Water Resources Research*, 53, 199– 221. https://doi.org/10.1002/2016WR019449

Doughty, C. (2007). Modeling geologic storage of carbon dioxide: Comparison of non-hysteretic and hysteretic characteristic curves. *Energy Conversion and Management*, 48(6), 1768– 1781. https://doi.org/10.1016/j.enconman.2007.01.022

Huppert, H. E., & Woods, A. W. (1995). Gravity-driven flows in porous media. *Journal of Fluid Mechanics*, 292(1), 55– 69. https://doi.org/10.1017/S0022112095001431

Juanes, R., Spiteri, E. J., Orr, F. M., & Blunt, M. J. (2006). Impact of relative permeability hysteresis on geological CO_2 storage. *Water Resources Research*, 42, W12418. https://doi.org/10.1029/2005WR004806

Klute, A., & Dirksen, C. (1986). Hydraulic conductivity and diffusivity, laboratory methods. In A. Klute (Ed.), *Methods of soil analysis. Part 1* (pp. 687– 732). Madison, WI: SSSA.

Liu, H. H., & Dane, J. H. (1995). Improved computational procedure for retention relations of immiscible fluids using pressure cells. *Soil Science Society of America Journal*, 59(6), 1520– 1524. https://doi.org/10.2136/sssaj1995.03615995005900060002x

Sakaki, T., & Illangasekare, T. H. (2007). Comparison of height-averaged and point-measured capillary pressure–saturation relations for sands using a modified Tempe cell. *Water Resources Research*, 43, W12502. https://doi.org/10.1029/2006WR005814

Tokunaga, T. K. (2009). Hydraulic properties of adsorbed water films in unsaturated porous media. *Water Resources Research*, 45, W06415. https://doi.org/10.1029/2009WR007734

Tokunaga, T. K., Wan, J., & Olson, K. R. (2002). Saturation-matric potential relations in gravel. *Water Resources Research*, 38(10), 1214. https://doi.org/10.1029/2001WR001242

Trevisan, L., Cihan, A., Agartan, E., Mori, H., Fagerlund, F., Birkholzer, J. T., et al. (2014). Investigation of mechanisms of supercritical CO_2 trapping in deep saline reservoirs using surrogate fluids at ambient laboratory conditions. *International Journal of Greenhouse Gas Control*, 29(C, 35– 49.

Trevisan, L., Pini, R., Cihan, A., Birkholzer, J. T., Zhou, Q., González-Nicolás, A., & Illangasekare, T. H. (2017). Imaging and quantification of spreading and trapping of carbon dioxide in saline aquifers using meter-scale laboratory experiments. *Water Resources Research*, 53, 485– 502. https://doi.org/10.1002/2016WR019749

Trevisan, L., Pini, R., Cihan, A., Birkholzer, J. T., Zhou, Q., & Illangasekare, T. H. (2015). Experimental analysis of spatial correlation effects on capillary trapping of supercritical CO_2 at the intermediate laboratory scale in heterogeneous porous media. *Water Resources Research*, 51, 8791– 8805. https://doi.org/10.1002/2015WR017440

Unsal, E., & Moulet-Vargas, E. (2013). Impact of wetting film flow in pore scale displacement, International Symposium of the Society of Core Analysts, SCA 2013–016.

United States Environmental Protection Agency (2008). Federal requirements under the Underground Injection Control (UIC) program for carbon dioxide (CO2) Geologic Sequestration (GS) wells, Proposed Rule, 40 CFR Parts 144 and 146, EPA-HQ-OW-2008–0390.

van der Marck, S. C. (1996). Network approach to void percolation in a pack of unequal spheres. *Physical Review Letters*, 77(9), 1785– 1788. https://doi.org/10.1103/PhysRevLett.77.1785

Zhang, Y., Shariati, M., & Yortsos, Y. C. (2000). The spreading of immiscible fluids in porous media under the influence of gravity. *Transport in Porous Media*, 38, 117– 140. https://doi.org/10.1023/A:1006663217326

Zhao, B., MacMinn, C. W., Huppert, H. E., & Juanes, R. (2014). Capillary pinning and blunting of immiscible gravity currents in porous media. *Water Resources Research*, 50, 7067– 7081. https://doi.org/10.1002/2014WR015335

Zhao, B., MacMinn, C. W., Szulczewski, M. L., Neufeld, J. A., Huppert, H. E., & Juanes, R. (2013). Interface pinning of immiscible gravity exchange flows in porous media. *Physical Review E*, 87(2), 023015. https://doi.org/10.1103/PhysRevE.87.023015